

Parameterizing DFT+U+V from Hybrid Functionals: A Wannier-Function-Based Approach for Strongly Correlated Materials

Dmitry M. Korotin,^{1,*} Anna A. Anisimova,¹ and Vladimir I. Anisimov^{1,2}

¹*M.N. Mikheev Institute of Metal Physics of the Ural Branch of the Russian Academy of Sciences,
18 S. Kovalevskaya St., Yekaterinburg, 620108, Russia*

²*Department of Theoretical Physics and Applied Mathematics,
Ural Federal University, 19 Mira St., Yekaterinburg 620002, Russia*

(Dated: February 25, 2026)

We present an approach to parameterize DFT+U+V from hybrid-functional calculations using Wannier-function projections. The method constructs a common localized Wannier basis for both semilocal DFT and hybrid-functional calculations, then determines effective on-site (U) and intersite (V) Hubbard parameters by minimizing the Hamiltonian mismatch within the correlated subspace. This procedure yields interaction parameters that reproduce the hybrid-functional electronic structure at a fraction of the computational cost and allow efficient structural relaxations and further many-body calculations. We validate the workflow on three oxide systems with different electronic characters: MgO (wide-gap insulator), NiO (antiferromagnetic charge-transfer insulator), and V₂O₅ (d⁰ transition-metal oxide). In all cases, the mapped DFT+U+V parameters reproduce hybrid-functional band gaps, densities of states, and magnetic moments and improve upon semilocal DFT while maintaining computational efficiency.

I. INTRODUCTION

Standard density functional theory (DFT) with local or semilocal exchange-correlation functionals (LDA/GGA) often fails to describe strongly correlated materials due to the inadequate treatment of electron-electron interactions. This leads to significant inaccuracies in predicting the electronic, magnetic, and structural properties of systems with partially filled d or f shells, such as transition-metal oxides, rare-earth compounds, and actinides. The DFT+ U method partially remedies this limitation by introducing a Hubbard-like correction that accounts for strong on-site Coulomb interactions between localized electrons [1–4]. This correction penalizes fractional occupations of localized orbitals, thereby reducing the self-interaction error inherent in conventional DFT and opening band gaps in systems incorrectly predicted to be metallic. The DFT+ V extension further improves the description by incorporating inter-site Coulomb interactions, which are particularly important in systems with significant charge transfer, orbital hybridization, or covalent bonding [5]. Together, the + U and + V corrections enhance the accuracy of DFT [6, 7] in describing charge localization, orbital ordering, magnetic properties, and band structures, while preserving its favorable computational scaling compared to more demanding many-body approaches such as GW or dynamical mean-field theory (DMFT) [8, 9].

A central challenge in applying DFT+ U and DFT+ V is choosing the Hubbard parameters U and V . These parameters are not fixed by the formalism and must be supplied externally. Two common strategies are (i) empirical tuning to reproduce selected experimental ob-

servables and (ii) first-principles estimates, for example from linear-response theory [10], constrained DFT [11], constrained random phase approximation (cRPA) [12], or the ACBN0 method [13, 14]. Empirical tuning is straightforward when reliable data are available, but it has limited predictive power and becomes impractical for systems or conditions without experimental reference data. First-principles approaches are more systematic and transferable, but they can be computationally demanding and sensitive to technical choices such as the basis set or supercell size. Moreover, inter-site interactions (V) are often neglected because they are more difficult to compute accurately.

Hybrid exchange–correlation functionals provide an alternative way to improve the description of localized electrons by mixing a fraction of exact exchange with a semilocal functional and, in screened/range-separated variants, attenuating the long-range part of the Fock term [15–18]. In many transition-metal oxides, this reduces self-interaction and improves the relative energetic alignment of ligand p and metal d states, leading to more realistic band gaps and magnetic moments compared to semilocal DFT.

The main limitation of hybrid functionals is the computational cost associated with evaluating the nonlocal exchange operator, which can become prohibitive for large cells, dense k -point meshes, or geometry optimization. Consequently, hybrids are often used as a reference for the electronic structure, while more affordable corrected semilocal approaches (e.g., DFT+ U + V) are preferred for extensive structural or configurational sampling.

The key idea of our approach is to use the accuracy of hybrid functionals in a computationally efficient framework by transferring their electronic structure information into a DFT+ U + V model. The method proceeds in four steps:

* dmitry@korotin.name

1. Calculate the electronic structure of the target compound using a hybrid functional.
2. Transform the hybrid-functional Bloch states into a localized Wannier representation and extract the corresponding Hamiltonian matrix elements within the correlated subspace.
3. Repeat the same procedure using a standard DFT functional (LDA/GGA), including the construction of the corresponding Wannier-function Hamiltonian.
4. Map the hybrid-functional Hamiltonian onto the DFT Hamiltonian augmented with DFT+ $U+V$ corrections, treating the interaction parameters as fitting variables.

In this way, one can obtain both (i) a set of localized basis functions [Wannier functions (WFs)] suitable for describing the low-energy electronic states near the Fermi level and (ii) the parameters of an extended Hubbard model, including inter-site interactions for an arbitrary number of coordination shells. These parameters can then be used in practical DFT+ $U+V$ calculations, for example for structural relaxations, and can also serve as input for more advanced electronic-structure approaches such as DFT+DMFT [8, 9] or for low-energy model analyses.

In this work, we test the proposed workflow on three oxides with different electronic structures: MgO, a wide-gap insulator without transition-metal ions for which semilocal DFT still underestimates the band gap; NiO, an antiferromagnetic charge-transfer insulator and a standard benchmark for correlation effects; and V₂O₅, a transition-metal oxide with a formally empty d shell (d^0) for which the DFT band gap is also substantially underestimated.

II. METHODS

A. Extraction of effective U and V parameters

We construct WFs by projecting the pseudoatomic orbitals onto a selected subspace of Bloch eigenstates and performing a Löwdin orthonormalization independently at each \mathbf{k} point. A detailed description of this procedure within the pseudopotential framework can be found in Ref. [19].

In reciprocal space, the projected WFs are

$$|W_{n\mathbf{k}}\rangle \equiv \sum_{\mu=N_1}^{N_2} |\Psi_{\mu\mathbf{k}}\rangle \langle \Psi_{\mu\mathbf{k}} | \phi_{n\mathbf{k}} \rangle. \quad (1)$$

Here, $\{|\Psi_{\mu\mathbf{k}}\rangle\}$ are Bloch eigenstates in the chosen band window from N_1 to N_2 . The resulting WFs are localized and retain the orbital character of the trial functions. The functions $|\phi_{n\mathbf{k}}\rangle$ are the Bloch sums of the corresponding pseudoatomic orbitals.

Real-space WFs are obtained by the Fourier transform

$$|W_n^{\mathbf{T}}\rangle = \frac{1}{\sqrt{N_{\mathbf{k}}}} \sum_{\mathbf{k}} e^{-i\mathbf{k}\cdot\mathbf{T}} |W_{n\mathbf{k}}\rangle, \quad (2)$$

where $N_{\mathbf{k}}$ is the number of \mathbf{k} points in the Brillouin-zone sampling.

To avoid ambiguity in real space, we use the following notation: i, j label atoms in the reference unit cell, \mathbf{T} is a Bravais-lattice translation vector, and $I \equiv (i, \mathbf{T}_I)$ labels a site in the replicated supercell (cluster). Orbital indices within the correlated shell on a given atom are denoted by m, n .

The matrix elements of the one-electron Hamiltonian in reciprocal space are defined as

$$H_{mn}^{\sigma}(\mathbf{k}) = \langle W_{m\mathbf{k}} | \left(\sum_{\mu=N_1}^{N_2} |\Psi_{\mu\mathbf{k}}\rangle \varepsilon_{\mu}^{\sigma}(\mathbf{k}) \langle \Psi_{\mu\mathbf{k}} | \right) | W_{n\mathbf{k}} \rangle, \quad (3)$$

where $\varepsilon_{\mu}^{\sigma}(\mathbf{k})$ is the eigenvalue of the one-electron Hamiltonian corresponding to band μ and spin σ .

The matrices $H^{\sigma}(\mathbf{k})$ are obtained in a post-processing step following the self-consistent cycle using the same WF projection procedure for both conventional DFT (denoted below as H^{DFT}) and hybrid-functional calculations (denoted as H^{hyb}).

The spin-resolved occupation matrix in the WF basis is defined as

$$n_{mn}^{\sigma}(\mathbf{k}) = \langle W_{m\mathbf{k}} | \left(\sum_{\mu=N_1}^{N_2} |\Psi_{\mu\mathbf{k}}\rangle f_{\mu}^{\sigma}(\mathbf{k}) \langle \Psi_{\mu\mathbf{k}} | \right) | W_{n\mathbf{k}} \rangle, \quad (4)$$

where $f_{\mu}^{\sigma}(\mathbf{k})$ is the occupation number (typically the Fermi-Dirac weight) of the Bloch state μ with spin σ and wavevector \mathbf{k} .

To determine the inter-site interaction parameters V , we require the Hamiltonian and occupation matrices between WFs centered on different atomic sites in real space. These quantities are obtained by Fourier transforming the \mathbf{k} -dependent WF matrices to real space and retaining the matrix elements corresponding to atoms located within a sphere of radius R_{cl} centered on a chosen reference correlated atom. This procedure defines an effective finite cluster in real space, without performing explicit supercell calculations.

For $X \in \{\text{DFT}, \text{hyb}\}$ we define

$$H_{mI, nJ, \sigma}^{X, \text{cl}} = \frac{1}{\sqrt{N_{\mathbf{k}}}} \sum_{\mathbf{k}} e^{-i\mathbf{k}\cdot(\mathbf{T}_J - \mathbf{T}_I)} H_{mn}^{X, \sigma}(\mathbf{k}),$$

$$n_{mI, nJ, \sigma}^{X, \text{cl}} = \frac{1}{\sqrt{N_{\mathbf{k}}}} \sum_{\mathbf{k}} e^{-i\mathbf{k}\cdot(\mathbf{T}_J - \mathbf{T}_I)} n_{mn}^{X, \sigma}(\mathbf{k}). \quad (5)$$

This procedure truncates inter-site interactions beyond R_{cl} . Although the screened exchange in hybrid functionals extends over a finite (but nonzero) spatial range, we

find that, for the systems studied here, the dominant contributions to V come from the first coordination shells where hybridization is strongest. Increasing R_{cl} mainly adds weak longer-range terms and only weakly changes the fitted on-site parameters and nearest-neighbor V values. Thus, the mapping captures the relevant part of the hybrid-functional interaction profile while remaining computationally tractable for practical DFT+ U + V applications.

In particular, Eq. (5) gives $H^{\text{DFT,cl}}$ and $H^{\text{hyb,cl}}$; the same notation is used for the occupation matrices $n^{\text{DFT,cl}}$ and $n^{\text{hyb,cl}}$.

Within this cluster basis, the DFT+ U + V correction to the one-electron Hamiltonian is written as

$$\Delta H_{mI,nJ}^{\sigma} = \delta_{IJ} U_I \left(\frac{1}{2} \delta_{mn} - n_{mI,nI,\sigma}^{\text{DFT,cl}} \right) - (1 - \delta_{IJ}) V_{IJ} n_{mI,nJ,\sigma}^{\text{DFT,cl}}. \quad (6)$$

Here, U_I is the on-site Hubbard parameter on site I and V_{IJ} is the inter-site interaction parameter for the pair of sites (I, J) .

The resulting effective Hamiltonian is

$$H_{\sigma}^{\text{model}} = H_{\sigma}^{\text{DFT,cl}} + \Delta H^{\sigma}(U, V). \quad (7)$$

The parameters $\{U_I\}$ and $\{V_{IJ}\}$ are determined by fitting $H_{\sigma}^{\text{model}}$ to the corresponding Hamiltonian obtained from hybrid-functional calculations, $H_{\sigma}^{\text{hyb,cl}}$. We minimize the following cost function:

$$\mathcal{L}(U, V) = \sum_{\sigma} \left\| H_{\sigma}^{\text{hyb,cl}} - (H_{\sigma}^{\text{DFT,cl}} + \Delta H^{\sigma}(U, V)) \right\|^2, \quad (8)$$

where the norm corresponds to the sum of squared differences between all matrix elements. Since $\Delta H^{\sigma}(U, V)$ depends linearly on the parameters, Eq. (8) reduces to a standard linear least-squares problem. In practice, only the independent (upper-triangular) matrix elements are included in the evaluation of Eq. (8), which avoids double counting due to hermiticity.

Equation (8) performs a least-squares fit of the full Wannier Hamiltonian matrix rather than only its eigenvalue spectrum. This procedure enforces agreement of both diagonal terms (level alignment and gaps) and off-diagonal terms (hybridization and effective hoppings) within the correlated subspace. As a result, the mapped parameters are better suited for subsequent structural relaxations and many-body extensions, where the full Hamiltonian matrix is required.

The fitted parameters depend on the definition of the correlated subspace, i.e., on the trial orbitals and the energy window used in the Wannier construction. Here we use Löwdin-orthonormalized projection Wannier functions, which fix the gauge in a transparent and reproducible way while preserving the symmetry and centers of the atomic-like trial orbitals. Within this choice, changing the energy window mainly changes the hybridization

with higher-lying states and can shift U and V quantitatively. We therefore treat the parameters as effective quantities defined for a specific low-energy manifold. When the window includes all states relevant near the Fermi level, the mapped Hamiltonian remains stable within that manifold.

B. Details of ground-state calculations

The electronic structure calculations were performed using the QUANTUM ESPRESSO package [20, 21]. Pseudopotentials were taken from the Standard Solid-State Pseudopotentials (SSSP) library, using the PBEsol Efficiency set (v1.3.0) [22] and the kinetic-energy cutoffs recommended by the authors for each element. Brillouin-zone integration was carried out on an $8 \times 8 \times 8$ Monkhorst–Pack k -point mesh in the irreducible Brillouin zone. Hybrid-functional calculations were performed using the HSE06 [15] hybrid functional with exact-exchange fraction $\alpha = 0.25$, based on the same structural model and \mathbf{k} -point mesh. The auxiliary \mathbf{q} -point grid used to evaluate the Fock exchange was set to $2 \times 2 \times 2$ for MgO, $4 \times 4 \times 4$ for NiO, and $2 \times 1 \times 4$ for V_2O_5 .

III. RESULTS

A. MgO

Magnesium oxide crystallizes in the rock-salt structure [23] and is a wide-gap insulator with an experimental gap of about 7.83 eV [24]. Even though it has no partially filled d or f shells, MgO is a useful benchmark because semilocal DFT still underestimates its gap [25, 26]. Using PBEsol, we obtained a band gap of 5.08 eV, while HSE06 yields 7.65 eV. We did not aim to reproduce the exact experimental gap; instead, we used the standard HSE06 parameters without tuning to test the proposed method. The DFT partial densities of states (PDOS) in the top panel of Fig. 1 show that states around the Fermi level have Mg s/p and O p character, consistent with appreciable Mg–O hybridization. Accordingly, we constructed Wannier functions for the Mg s and p states and for the O p states, spanning an energy window from -8 eV to 20 eV relative to the Fermi level.

The mapping yielded the following on-site parameters: $U_{\text{Mg } s} = 1.05$ eV, $U_{\text{Mg } p} = 0.44$ eV, and $U_{\text{O } p} = 5.80$ eV. For the inter-site terms, we obtained $V_{\text{Mg } s-\text{O } p} = 1.96$ eV and $V_{\text{Mg } p-\text{O } p} = 1.98$ eV.

Figure 1 compares the PDOS obtained using DFT (PBEsol), the HSE06 hybrid functional, and DFT+ U + V with the mapped parameters. The DFT+ U + V calculation increases the band gap to 7.05 eV, bringing it closer to both the HSE06 result and experiment. Moreover, the overall PDOS shape obtained within DFT+ U + V closely follows that of the hybrid-functional calculation.

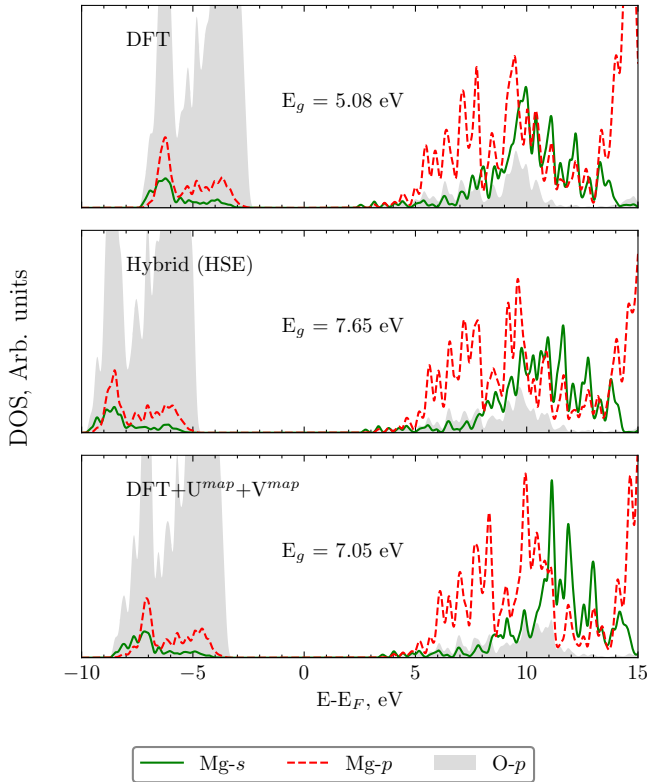


Figure 1. Projected density of states of MgO calculated using DFT (PBEsol), the HSE06 hybrid functional, and DFT+ $U+V$ with parameters fitted from HSE06.

An exact match between the DFT+ $U+V$ and HSE06 band gaps is not expected. One reason is that the correlated subspace differs between the two approaches. In the hybrid-functional calculation, all valence and conduction states are treated on an equal footing, whereas in DFT+ $U+V$ only a selected subset of states is explicitly corrected. In addition, for simplicity, we included only the first shell of nearest neighbors when evaluating the inter-site parameters V for MgO. These differences lead to small residual discrepancies in the resulting band gaps.

Large Hubbard interactions on oxygen p orbitals are not merely a methodological artifact. Recent estimates based on the constrained random-phase approximation (cRPA) and related schemes report effective U_{pp} values of several electron-volts (typically 5–8 eV) [27, 28] for a broad class of oxides, including both Mott–Hubbard and charge-transfer insulators. These values are comparable to typical U_{dd} or U_{ff} parameters and reflect the finite localization of oxygen p states and incomplete screening in oxides, rather than an “overcorrection” for nominally filled bands.

B. NiO

Nickel oxide is a prototypical strongly correlated material with antiferromagnetic (AFM) order. It is a charge-transfer insulator where the band gap opens between oxygen p states and nickel d states [29]. NiO is therefore a standard benchmark for beyond-DFT methods used to improve band gaps and magnetic moments compared with semilocal DFT [1, 5, 30–32].

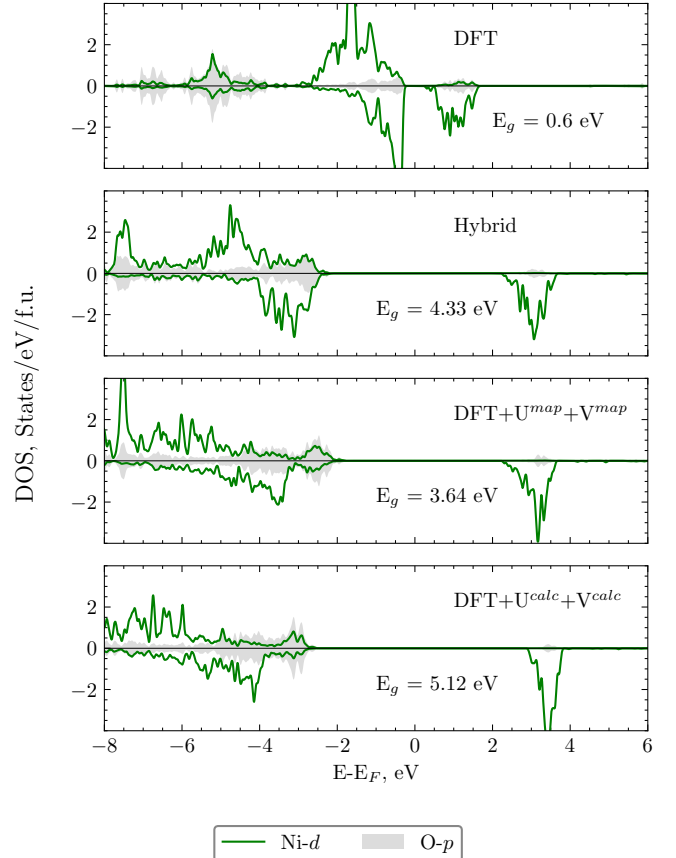


Figure 2. Projected density of states of NiO calculated using DFT (PBEsol), the HSE06 hybrid functional, DFT+ $U^{map}+V^{map}$ with parameters mapped from HSE06, and DFT+ $U^{calc}+V^{calc}$ with parameters from linear-response theory. The positive and negative values of the vertical axis correspond to spin-up and spin-down channels, respectively.

The PDOS of NiO calculated using DFT (PBEsol) and HSE06 are shown in the top two panels of Fig. 2. PBEsol yields a band gap of 0.6 eV, which strongly underestimates the experimental value of 3.7–4.3 eV [29, 33]. In contrast, HSE06 predicts a band gap of 4.33 eV, in agreement with experiment.

To construct the correlated subspace for NiO, we included the Ni $3d$ and O $2p$ states, which are essential for capturing the charge-transfer nature of the band gap. The Wannier functions were generated by projection onto these atomic-like orbitals within an energy window from -8 eV to 5 eV relative to the Fermi level.

The mapping yielded $U_{\text{Ni}3d} = 6.75$ eV and $U_{\text{O}2p} = 2.64$ eV for the on-site interactions, and $V_{\text{Ni}3d-\text{O}2p} = 1.54$ eV and $V_{\text{O}2p-\text{O}2p} = 1.84$ eV for the inter-site interactions. The third panel in Fig. 2 shows the PDOS obtained using DFT+ $U+V$ with the mapped parameters. The calculated band gap is 3.64 eV, close to the HSE06 reference and in good agreement with experiment. The overall PDOS shape also aligns well with that of the hybrid-functional calculation.

We also computed the extended-Hubbard parameters for NiO using linear-response theory [34]. The obtained values are $U_{\text{Ni}3d} = 7.61$ eV, $U_{\text{O}2p} = 9.69$ eV, and $V_{\text{Ni}3d-\text{O}2p} = 0.19$ eV. These are consistent with the values reported in Ref. [35]. The PDOS obtained using DFT+ $U+V$ with these parameters is shown in the bottom panel of Fig. 2. The calculated band gap is 5.12 eV, which overestimates both the HSE06 result and experiment. This discrepancy is consistent with the larger U values for the Ni d and O $2p$ states obtained from linear response compared to those derived from the mapping procedure.

In addition to the band gap, we compare the Ni magnetic moment estimated from Löwdin charges for the four approaches considered here (Table I). The PBEsol value ($1.32 \mu_B$) is substantially smaller than that obtained with HSE06 ($1.71 \mu_B$). The DFT+ $U^{map}+V^{map}$ result ($1.69 \mu_B$) is close to the hybrid-functional reference, whereas DFT+ $U^{calc}+V^{calc}$ yields a slightly larger moment ($1.83 \mu_B$), consistent with the overestimation of the band gap in that setup.

Table I. Ni magnetic moment obtained from Löwdin charges for NiO calculated using PBEsol, HSE06, DFT+ $U^{map}+V^{map}$ with parameters mapped from HSE06, and DFT+ $U^{calc}+V^{calc}$ with parameters from linear-response theory.

Method	$\mu_{\text{Ni}} (\mu_B)$
PBEsol	1.32
HSE06	1.71
DFT+ $U^{map}+V^{map}$	1.69
DFT+ $U^{calc}+V^{calc}$	1.83

All approaches considered here slightly underestimate the experimental Ni magnetic moment of $1.90 \mu_B$ [36]. This residual discrepancy can be attributed to (i) the finite Wannier projection window, (ii) the absence of dynamical correlations beyond static DFT+ $U+V$ or hybrid exchange, and (iii) the sensitivity of local moments to the balance between U and V , which controls the degree of $p-d$ hybridization. Nevertheless, the mapped DFT+ $U+V$ parameters reproduce the hybrid-functional moment closely, indicating that spin polarization is captured within the chosen low-energy subspace.

C. V_2O_5

Vanadium pentoxide (V_2O_5) is a layered transition-metal oxide that is often described as a d^0 system with nominally empty V $3d$ states. Because vanadium is in a high oxidation state, the hybridization between V- d and O- p states is substantial. Experimentally, the band gap of $\alpha\text{-V}_2\text{O}_5$ is 2.5 eV [37]. Despite the absence of partially filled d shells, semilocal DFT typically underestimates the gap and can misplace the V $3d$ conduction-band manifold relative to the O $2p$ valence states. For this reason, additional treatments of Coulomb interactions are often used to describe V_2O_5 properties [38, 39]. This makes V_2O_5 a useful test case for the present mapping strategy: it probes whether the fitted U and V parameters can reproduce a hybrid-functional reference even when correlation effects are not primarily of the Mott-Hubbard type.

Following the same procedure as for MgO and NiO, we first computed the electronic structure of V_2O_5 using PBEsol and HSE06. PBEsol underestimates the band gap (1.83 eV), while HSE06 yields a larger (overestimated) value of 3.43 eV. The hybrid gap could be tuned by changing the fraction of exact exchange, but we did not pursue this here because our goal is to validate the mapping approach.

To construct the correlated subspace, we included the V $3d$ and O $2p$ orbitals, which provide a compact description of the states near the valence-band maximum and the conduction-band minimum. We generated Wannier functions by projection onto these atomic-like orbitals within an energy window that captures the full O $2p$ valence manifold and the low-lying V $3d$ conduction states, from -7 eV to 6 eV relative to the Fermi level.

The mapping yields the parameters summarized in Table II, together with the linear-response values used in the DFT+ $U^{calc}+V^{calc}$ calculations. Since V_2O_5 contains three inequivalent oxygen sites, the interaction parameters differ slightly among them.

Table II shows that the two parameterization strategies yield systematically different interaction strengths. The on-site terms obtained from linear response are substantially larger than the mapped values (by roughly a factor of 2–3 for both V- $3d$ and O- $2p$). The inter-site terms show a less uniform trend: the mapped V–O interactions are generally larger than their linear-response counterparts. For O–O interactions, the two approaches yield values of the same order of magnitude (where both are available), and these remain below the on-site values in both approaches. In the mapped dataset, the inter-site interactions tend to decrease with increasing interatomic separation, consistent with the finite range of the dominant hybridization paths.

Figure 3 summarizes the PDOS obtained with semilocal DFT (PBEsol), the HSE06 hybrid functional, and DFT+ $U+V$ calculations. In agreement with the formal d^0 configuration, the valence-band manifold is dominated by O- p states, whereas the conduction-band edge has

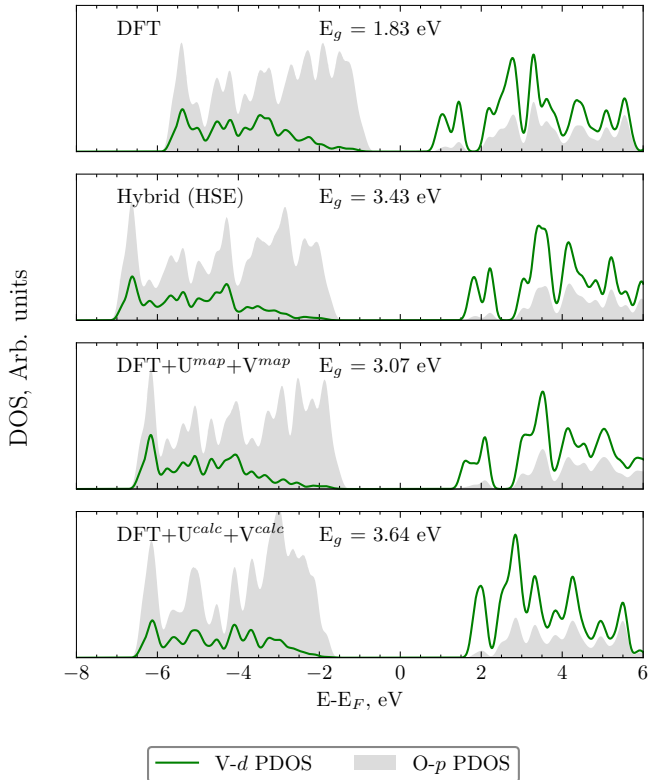


Figure 3. Projected density of states of V_2O_5 calculated using DFT (PBEsol), the HSE06 hybrid functional, DFT+ U^{map} + V^{map} with parameters mapped from HSE06, and DFT+ U^{calc} + V^{calc} with parameters from linear-response theory. The green and gray curves correspond to the V- d and O- p contributions, respectively.

strong V- d character.

With the mapped parameters, the DFT+ U^{map} + V^{map} calculation opens the band gap to 3.07 eV and reproduces the main features of the hybrid-functional PDOS. For comparison, DFT+ U^{calc} + V^{calc} yields a gap of 3.64 eV, which is slightly larger than the HSE06 reference and deviates further from the experimental value of 2.5 eV.

IV. CONCLUSION

We introduce a Wannier-function-based scheme to extract DFT+ U + V parameters from a hybrid-functional reference by matching the one-electron Hamiltonians in a common localized basis. The on-site and inter-site interaction parameters are obtained by minimizing the difference between the hybrid-functional Hamiltonian and a DFT Hamiltonian supplemented with U and V corrections within a selected Wannier subspace. The resulting parameters are effective quantities that depend on the chosen Wannier representation rather than unique, universally transferable interaction strengths.

An important practical benefit is that the approach provides both a well-defined localized basis and a consis-

Table II. Mapped (from HSE06) and linear-response-derived interaction parameters for V_2O_5 . The distance column is given only for inter-site terms.

Parameter	Mapped (eV)	LR (eV)	Inter-site distance (\AA)
$U_{V\ 3d}$	2.19	5.54	—
$U_{O1\ 2p}$	2.62	7.57	—
$U_{O2\ 2p}$	2.64	7.61	—
$U_{O3\ 2p}$	2.40	7.22	—
$V_{V\ 3d-O1\ 2p}$	1.93	0.67	1.58
$V_{V\ 3d-O2\ 2p}$	1.80	1.01	1.88
$V_{V\ 3d-O2\ 2p}$	1.86	1.01	2.02
$V_{V\ 3d-O3\ 2p}$	1.83	0.95	1.78
$V_{O1\ 2p-O2\ 2p}$	1.10	0.59	2.74
$V_{O1\ 2p-O2\ 2p}$	1.13	0.59	2.87
$V_{O1\ 2p-O3\ 2p}$	1.11	0.53	2.65
$V_{O3\ 2p-O2\ 2p}$	1.29	0.68	2.74
$V_{O3\ 2p-O2\ 2p}$	0.81	0.68	3.67
$V_{O2\ 2p-O2\ 2p}$	1.61	—	2.39

tent set of extended Hubbard parameters for that basis. Because the mapping is performed on the full Hamiltonian matrix, it preserves not only band gaps but also the off-diagonal elements that encode orbital hybridization and inter-site coupling, which are essential for subsequent structural or many-body calculations.

We tested the method on three representative oxides—MgO, NiO, and V_2O_5 . In all three cases, the mapped parameters lead to DFT+ U + V electronic structures that are much closer to the hybrid-functional results than standard semilocal DFT. In MgO, the correction mainly shifts the O-2 p states relative to Mg-derived states, resulting in a band gap close to that of HSE06. In NiO, treating both Ni-3 d and O-2 p states within the correlated subspace reproduces the charge-transfer gap and the magnetic moment of the hybrid-functional reference. In V_2O_5 , where the states are strongly hybridized despite the formal d^0 configuration, the mapping reduces the on-site U values but increases inter-site V terms, leading to improved agreement with the hybrid-functional density of states than parameters obtained from linear response.

The extracted U and V values depend on the Wannier energy window, the projection scheme, and the real-space cutoff used to define the interaction cluster. This dependence is inherent to any low-energy mapping because different subspaces capture different aspects of the electronic structure. Nevertheless, when the Wannier window consistently includes all states relevant near the Fermi level, the present approach yields stable parameters suitable for DFT+ U + V calculations.

The method provides a computationally efficient way to transfer the improved electronic-structure description of hybrid functionals into a semilocal DFT+ U + V framework suitable for large-scale simulations and structural optimization.

ACKNOWLEDGMENTS

The Hubbard model parameter mapping procedure was developed with support from the Russian Science Foundation (Project 24-12-00024). The linear-response calculations were supported by the Ministry of Science and Higher Education of the Russian Federation.

DATA AVAILABILITY

The data supporting the findings of this study are available from the corresponding author upon reason-

able request. All calculations were performed using publicly available electronic-structure codes, and the computational parameters required to reproduce the results are provided in the Methods section. The Python code used to fit the Wannier-function Hamiltonian matrices and extract the effective Hubbard parameters is openly available at <https://github.com/dkorotin/UVextract>.

-
- [1] V. I. Anisimov, J. Zaanen, and O. K. Andersen, Band theory and Mott insulators: Hubbard U instead of Stoner I, *Physical Review B* **44**, 943 (1991).
- [2] A. I. Liechtenstein, V. I. Anisimov, and J. Zaanen, Density-functional theory and strong interactions: Orbital ordering in Mott-Hubbard insulators, *Phys. Rev. B* **52**, R5467 (1995).
- [3] S. L. Dudarev, G. A. Botton, S. Y. Savrasov, C. J. Humphreys, and A. P. Sutton, Electron-energy-loss spectra and the structural stability of nickel oxide: An LSDA+U study, *Phys. Rev. B* **57**, 1505 (1998).
- [4] V. I. Anisimov, F. Aryasetiawan, and A. I. Liechtenstein, First-principles calculations of the electronic structure and spectra of strongly correlated systems: The LDA+U method, *Journal of Physics: Condensed Matter* **9**, 767 (1997).
- [5] V. Leiria Campo Jr and M. Cococcioni, Extended DFT + U + V method with on-site and inter-site electronic interactions, *Journal of Physics: Condensed Matter* **22**, 055602 (2010).
- [6] I. Timrov, F. Aquilante, M. Cococcioni, and N. Marzari, Accurate electronic properties and intercalation voltages of olivine-type li-ion cathode materials from extended hubbard functionals, *PRX Energy* **1**, 033003 (2022).
- [7] C. Ricca, I. Timrov, M. Cococcioni, N. Marzari, and U. Aschauer, Self-consistent DFT+ $u+v$ study of oxygen vacancies in srTiO_3 , *Phys. Rev. Res.* **2**, 023313 (2020).
- [8] A. Georges, G. Kotliar, W. Krauth, and M. J. Rozenberg, Dynamical mean-field theory of strongly correlated fermion systems and the limit of infinite dimensions, *Rev. Mod. Phys.* **68**, 13 (1996).
- [9] G. Kotliar, S. Y. Savrasov, K. Haule, V. S. Oudovenko, O. Parcollet, and C. A. Marianetti, Electronic structure calculations with dynamical mean-field theory, *Rev. Mod. Phys.* **78**, 865 (2006).
- [10] M. Cococcioni and S. de Gironcoli, Linear response approach to the calculation of the effective interaction parameters in the LDA+U method, *Phys. Rev. B* **71**, 035105 (2005).
- [11] V. I. Anisimov and O. Gunnarsson, Density-functional calculation of effective coulomb interactions in metals, *Phys. Rev. B* **43**, 7570 (1991).
- [12] F. Aryasetiawan, M. Imada, A. Georges, G. Kotliar, S. Biermann, and A. I. Liechtenstein, Frequency-dependent local interactions and the Calculations of correlated systems, *Phys. Rev. B* **70**, 195104 (2004).
- [13] L. A. Agapito, S. Curtarolo, and M. Buongiorno Nardelli, Reformulation of DFT + U as a Pseudohybrid Hubbard Density Functional for Accelerated Materials Discovery, *Physical Review X* **5**, 011006 (2015).
- [14] N. Tancogne-Dejean and A. Rubio, Parameter-free hybridlike functional based on an extended Hubbard model: DFT + U + V, *Physical Review B* **102**, 155117 (2020).
- [15] J. Heyd, G. E. Scuseria, and M. Ernzerhof, Hybrid functionals based on a screened Coulomb potential, *The Journal of Chemical Physics* **118**, 8207 (2003).
- [16] J. Heyd, G. E. Scuseria, and M. Ernzerhof, Erratum: Hybrid functionals based on a screened Coulomb potential [*J. Chem. Phys.* 118, 8207 (2003)], *The Journal of Chemical Physics* **124**, 219906 (2006).
- [17] C. Adamo and V. Barone, Toward reliable density functional methods without adjustable parameters: The PBE0 model, *The Journal of Chemical Physics* **110**, 6158 (1999).
- [18] A. D. Becke, Density-functional thermochemistry. III. the role of exact exchange, *The Journal of Chemical Physics* **98**, 5648 (1993).
- [19] Dm. Korotin, A. V. Kozhevnikov, S. L. Skornyakov, I. Leonov, N. Binggeli, V. I. Anisimov, and G. Trimarchi, Construction and solution of a Wannier-functions based Hamiltonian in the pseudopotential plane-wave framework for strongly correlated materials, *The European Physical Journal B* **65**, 91 (2008).
- [20] P. Giannozzi, S. Baroni, N. Bonini, M. Calandra, R. Car, C. Cavazzoni, D. Ceresoli, G. L. Chiarotti, M. Cococcioni, I. Dabo, A. Dal Corso, S. de Gironcoli, S. Fabris, G. Fratesi, R. Gebauer, U. Gerstmann, C. Gougoussis, A. Kokalj, M. Lazzeri, L. Martin-Samos, N. Marzari, F. Mauri, R. Mazzarello, S. Paolini, A. Pasquarello, L. Paulatto, C. Sbraccia, S. Scandolo, G. Sclauzero, A. P. Seitsonen, A. Smogunov, P. Umari, and R. M. Wentzcovitch, QUANTUM ESPRESSO: A modular and open-source software project for quantum simulations of materials, *Journal of Physics: Condensed Matter* **21**, 395502 (2009).
- [21] P. Giannozzi, O. Baseggio, P. Bonfà, D. Brunato, R. Car, I. Carnimeo, C. Cavazzoni, S. de Gironcoli, P. Delugas, F. Ferrari Ruffino, A. Ferretti, N. Marzari, I. Timrov, A. Urru, and S. Baroni, Quantum ESPRESSO toward the exascale, *The Journal of Chemical Physics* **152**, 154105 (2020).

- (2020).
- [22] G. Prandini, A. Marrazzo, I. E. Castelli, N. Mounet, and N. Marzari, Precision and efficiency in solid-state pseudopotential calculations, *npj Computational Materials* **4**, 72 (2018).
- [23] M. I. McCarthy and N. M. Harrison, Ab initio determination of the bulk properties of mgo, *Phys. Rev. B* **49**, 8574 (1994).
- [24] R. Whited, C. J. Flaten, and W. Walker, Exciton thermoreflectance of mgo and cao, *Solid State Communications* **13**, 1903 (1973).
- [25] J. Yang, S. Falletta, and A. Pasquarello, Range-separated hybrid functionals for accurate prediction of band gaps of extended systems, *npj Computational Materials* **9**, 108 (2023).
- [26] M. Großmann, M. Thieme, M. Grunert, and E. Runge, Many-body perturbation theory vs. density functional theory: a systematic benchmark for band gaps of solids, *npj Computational Materials* **12**, 10.1038/s41524-025-01855-4 (2026).
- [27] C. Ezeakunne, B. Lamichhane, and S. Kattel, Integrating density functional theory with machine learning for enhanced band gap prediction in metal oxides, *Physical Chemistry Chemical Physics* **27**, 5338 (2025).
- [28] R. Outerovitch and B. Amadon, Electronic interaction U p p on oxygen p orbitals in oxides: Role of correlated orbitals on the example of UO₂ and TiO₂, *Physical Review B* **107**, 235126 (2023).
- [29] G. A. Sawatzky and J. W. Allen, Magnitude and origin of the band gap in nio, *Phys. Rev. Lett.* **53**, 2339 (1984).
- [30] J. Kuneš, V. I. Anisimov, a. V. Lukoyanov, and D. Vollhardt, Local correlations and hole doping in NiO: A dynamical mean-field study, *Physical Review B* **75**, 4 (2007).
- [31] O. Bengone, M. Alouani, P. Blöchl, and J. Hugel, Implementation of the projector augmented-wave lda+u method: Application to the electronic structure of nio, *Phys. Rev. B* **62**, 16392 (2000).
- [32] M. J. DelloStritto, A. D. Kaplan, J. P. Perdew, and M. L. Klein, Predicting the properties of NiO with density functional theory: Impact of exchange and correlation approximations and validation of the r2SCAN functional, *APL Materials* **11**, 060702 (2023).
- [33] R. J. Powell and W. E. Spicer, Optical Properties of NiO and CoO, *Physical Review B* **2**, 2182 (1970).
- [34] I. Timrov, N. Marzari, and M. Cococcioni, HP – A code for the calculation of Hubbard parameters using density-functional perturbation theory, *Computer Physics Communications* **279**, 108455 (2022).
- [35] L. F. Garcia-Uc, J. Hernández-Tecorralco, and R. De Coss, Chemical bond and intersite Hubbard corrections in NiO and TiO₂: A self-consistent DFT + U + V study, *Computational Materials Science* **261**, 114337 (2026).
- [36] A. K. Cheetham and D. A. O. Hope, Magnetic ordering and exchange effects in the antiferromagnetic solid solutions Mn_xNi_{1-x}O, *Physical Review B* **27**, 6964 (1983).
- [37] Z. Bodó and I. Hevesi, Optical Absorption near the Absorption Edge in V₂O₅ Single Crystals, *physica status solidi (b)* **20**, 10.1002/pssb.19670200153 (1967).
- [38] E. M. Roginskii, M. B. Smirnov, K. S. Smirnov, R. Baddour-Hadjean, J.-P. Pereira-Ramos, A. N. Smirnov, and V. Y. Davydov, A Computational and Spectroscopic Study of the Electronic Structure of V₂O₅-Based Cathode Materials, *The Journal of Physical Chemistry C* **125**, 5848 (2021).
- [39] Y. Plotnikov and Dm.M. Korotin, Electronic correlation effects on zinc-ion migration in V₂O₅: A DFT+ U study, *Journal of Physics and Chemistry of Solids* **208**, 113172 (2026).